Polymer 51 (2010) 738–747

Contents lists available at ScienceDirect

Polymer

journal homepage: www.elsevier.com/locate/polymer

Effects of chain conformation on miscibility, morphology, and mechanical properties of solution blended substituted polyphenylene and polyphenylsulfone

Paul J. Jones, Lea C. Paslay, Sarah E. Morgan*

School of Polymers and High Performance Materials, University of Southern Mississippi, Hattiesburg, MS 39406, USA

ARTICLE INFO

Article history:
Received 19 August 2009
Received in revised form
6 December 2009
Accepted 9 December 2009
Available online 21 December 2009

Keywords:
Polyphenylene
Polyphenylsulfone
Molecular composites

ABSTRACT

The effects of polymer conformation and degree of substitution on miscibility, morphology and mechanical properties of solution blended systems containing polyphenylsulfone and copolymers of phenylketone substituted *p*-phenylene with *m*-phenylene were studied. Static and dynamic light scattering studies were performed to obtain the *z*-average root mean square radius of gyration, second virial coefficient, weight average molecular weight and hydrodynamic radius. Solution blends of polyphenylsulfone with phenylene copolymers yielded free standing films. Blend miscibility was assessed by glass transition behavior, morphology was analyzed using atomic force microscopy and mechanical properties were measured using nanoindentation. Copolymer composition determined miscibility. Miscible blends exhibited homogeneous morphologies while immiscible blends displayed unique, heterogeneous morphologies. Polymer conformation in solution, rather than enthalpic contributions, was the primary determinant of miscibility. Successful reinforcement was achieved in blended systems.

1. Introduction

Molecular composites are blends containing rigid-rod polymers that act as reinforcing agents dispersed within a flexible polymer matrix. When no interface exists between the reinforcing fibers and the polymer matrix, molecular composites can also be referred to as homogeneous composites [1]. According to composite theory, successful mechanical reinforcement is described by the rule of mixtures and occurs when the aspect ratio of the reinforcing component is greater than one hundred [2]. Development of molecular composites has the potential to provide new materials with increased strength to weight ratios and improved dimensional and thermal stabilities. Composite performance is driven by the molecular level reinforcing agent and its interaction with the matrix [3,4]. A primary challenge in developing useful composites of this type is the dispersion of the rigid-rod polymer within the flexible matrix. Unlike blends of coiled polymers where compatibility can be achieved by offsetting an unfavorable enthalpy of mixing with a favorable entropy of mixing, blends containing rigid-rod and coiled polymers most often suffer from a highly unfavorable mixing entropy due to differences in conformation. As a result of steric forces, rigid-rod polymers form an ordered phase, excluding the coiled polymers. This effect, commonly referred to as entropic demixing, most often leads to unstable or incompatible blends even when favorable enthalpy of mixing exists between the rigid-rod and coiled polymers [5–7]. In order to create a molecular composite, the thermodynamic effects of entropic demixing must be counteracted by altering the rigid-rod polymer to allow incorporation of the coiled polymer in the rigid phase [8–11]. Increasing the free volume associated with the rigid-rod phase has been shown to relax the steric constraints and inhibit the formation of an ordered state [12]. Effective methods for increasing free volume include modification of the rigid-rod polymer through side group attachment and introduction of nonlinear monomers into the polymer backbone [12].

The rigid-rod polyphenylenes investigated in this study are copolymers of *para*-phenylene substituted by a phenylketone group and *meta*-phenylene, with the generalized structure shown in Fig. 1. These transparent, amorphous polymers have been classified as self reinforcing polymers (SRPs) for their high strength and modulus without the addition of reinforcing agents [13,14]. SRPs are inherently both thermally and dimensionally stable and have been shown to possess mechanical properties far superior to known high performance thermoplastics [15–17]. Their mechanical performance makes them excellent candidates as reinforcing elements when blended with flexible polymers. Miscible blends of this nature are classified as molecular composites. Although SRPs have typically exhibited low melt compatibility with other polymers, high levels of miscibility have been reported for SRP/polyetherimide (PEI) blends [18]. Studies of tertiary melt blends

* Corresponding author. Tel.: +1 601 818 6728; fax: +1 601 266 5635.
E-mail address: sarah.morgan@usm.edu (S.E. Morgan).

0032-3861/$ – see front matter © 2009 Elsevier Ltd. All rights reserved.
doi:10.1016/j.polymer.2009.12.010

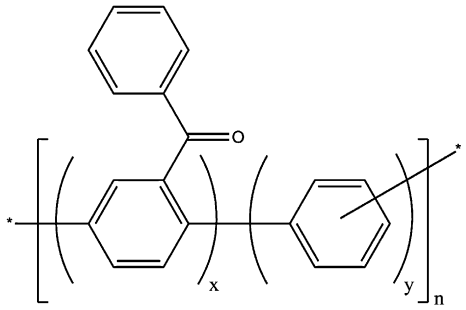

Fig. 1. Generalized chemical structure of SRP copolymer.

containing SRP, polyetheretherketone (PEEK), and polyphenylsulfone (PPSU) demonstrated that PPSU increases compatibility between SRP and PEEK [19]. While less industrially viable, solution blending provides a more effective means for creating homogeneous blends of SRPs. Solution blends of SRP with polyimide, polycarbonate, and polysulfone yielded transparent films [15,20]. Formation of optically clear films provides evidence of blend miscibility, but complicated processes that occur during solution casting often alter the state of mixing. Deviation from a state of thermodynamic equilibrium in solution cast films is due to the diffusion kinetics of the polymers in solution, the solubility of the polymers in solution and the surface free energy of the blend components. Non-homogenous films can be produced from polymers that usually form miscible blends if the solution becomes trapped in a state of immiscibility based on the tertiary solvent–polymer–polymer phase diagram [21,22]. Conversely, a homogeneous film can be produced from immiscible polymers if the solvent is removed at such a rate that the polymers cannot kinetically diffuse into a state of thermodynamic equilibrium before solidification occurs [23]. Immiscible polymer blends will often display an enrichment of one component at the surface. Typically, the component with the lower surface free energy will be enriched at the surface in order to minimize polymer-air surface tension, and the component with the lower solubility will deposit on the substrate first due to solvent effects [24].

In this study, solution blends of two SRP copolymers with PPSU and their films are investigated to determine miscibility and molecular reinforcement properties. Static and dynamic light scattering techniques are used to obtain information about the physical dimensions and intermolecular interactions of the two different SRP copolymers and polyphenylsulfone (PPSU) in solution. Surface free energies are measured using contact angle goniometry. Miscibility is characterized by observing the glass transition behavior of the blends, and the morphology is imaged by atomic force microscopy (AFM). The mechanical performance of the blends is assessed using nanoindentation and compared to the upper limit of mechanical reinforcement predicted by the rule of mixtures.

2. Experimental

2.1. Materials

PPSU and two variations of SRP (SRP-A and SRP-B) were supplied by Solvay Advanced Polymers, L.L.C. in powder form. The SRPs are copolymers of phenylketone substituted *para*-phenylene with *meta*-phenylene. SRP-A contains a low amount (less than 25 mol%) of m-phenylene recurring units, and SRP-B contains a higher amount of m-phenylene (40–60 mol%). Both copolymers are commercially available under the trade name PRIMOSPIRE® [17]. The reported tensile moduli for SRP-A and SRP-B are 8.3 and 5.5 GPa, respectively. PPSU has a reported tensile modulus of 2.3 GPa [25]. Anhydrous 1-methyl-2-pyrrolidone (NMP), anhydrous toluene, and a 5000 molecular weight polystyrene standard were obtained from Sigma–Aldrich. Anhydrous solvents were supplied in sealed bottles and only opened immediately prior to solution preparation. In each case that a polymer solution or solvent was filtered, an inorganic membrane filter (Anotop 25, Whatman, Maidstone, UK) was used.

2.2. Sample preparation

For light scattering measurements all glassware was rinsed with filtered ethanol and dried prior to use to remove any dust collected. Polymer powders were dried in a vacuum oven at 120 °C for 1 h prior to dissolution. Stock solutions were prepared by adding 1 g of dry polymer to a 100 mL volumetric flask. NMP is a hygroscopic solvent, and precautions were taken to minimize water absorption by limiting its exposure to the laboratory environment. To remove dust NMP was drawn from a sealed container into a syringe and then added to the flask through a 0.02 μm pore size filter. The polymers were dissolved under nitrogen. The stock solution was added to a scintillation vial through a 0.2 μm pore size filter and diluted solutions were prepared by adding NMP to the same vial through a 0.02 μm pore size filter. Using the same scintillation vial to dilute a polymer solution during light scattering minimizes error due to variations in the scintillation vial since it also serves as the measurement chamber during batch measurements. The least concentrated polymer solutions used during static light scattering (SLS) measurements were used for dynamic light scattering (DLS) measurements. Each solution was stored in a desiccation chamber after preparation.

Solution cast polymer films were prepared by mixing stock solutions at 10 wt% in different ratios to make blended solutions. The blended solutions were applied to glass plates and placed into a vacuum oven at 30 °C and an absolute pressure of approximately 20 kPa to prevent rapid flashing of the solvent. The temperature was increased at a rate of 30 °C per hour until 150 °C was reached. Pressure was gradually reduced each time the temperature was increased until the maximum vacuum was achieved around 1–2 kPa. The films were left in the vacuum oven overnight and placed in a convection oven at 205 °C for 1 h to remove any remaining solvent.

2.3. Light scattering

The *z*-average root mean square radius of gyration ($<R_G>_z$), weight average molecular weight (M_w), and second virial coefficient (A_2) of the polymers in NMP were measured by SLS techniques using a multi-angle photometer DAWN DSP (Wyatt Technologies Corp, Santa Barbara, CA) in batch mode. This instrument uses a He–Ne laser with wavelength (λ) of 632.8 nm as the excitation source. Scintillation vials served as the batch cell, and 11 fixed angle detectors between 44° and 147° were used to collect the scattered light. An absolute calibration of the photometer was carried out using anhydrous toluene filtered through a 0.02 μm pore size filter into a clean scintillation vial. The individual photodiodes were normalized using an isotropic scattering solution. The isotropic scattering solution was a narrow molecular weight polystyrene standard (most probable molecular weight of 5000) in toluene. Polystyrene having this molecular weight in toluene has a radius of gyration (R_G) of approximately 2.3 nm and behaves as an isotropic light scattering solution. The differential refractive index of each polymer in NMP was measured by a refractometer (Bausch and Lomb), and NMP filtered through a 0.02 μm pore size filter was used to establish the baseline. SLS data is linearly fitted using Zimm formalism, where K^*c/R_{theta} is plotted versus $\sin^2(\text{theta}/2)$. K is an

optical constant, c is solution concentration in g/mL, R_{theta} is Rayleigh's ratio, and theta is the scattering angle. In each figure the data is extrapolated to both theta = 0° and $c = 0$. The inverse of the intercept of each extrapolated line is the weight average molecular weight, M_w. The limiting slope of the line projected to theta = 0° at constant c gives the second virial coefficient (A_2). Due to the polydisperse nature of the polymers investigated the limiting slope of the line projected to $c = 0$ at constant theta gives the z-average root mean square radius of gyration $<R_g^2>_z$ [26,27]. The relationship between R_G^2 and $<R_G^2>_z$ is given by Eq. (1).

$$\left\langle R_G^2 \right\rangle_Z = \sum_i w_i M_i R_G^2(i) / \sum_i w_i M_i \tag{1}$$

The hydrodynamic radii (R_h) of the polymers in NMP were measured by DLS using a Malvern Instruments Zetasizer Nano series instrument equipped with a He–Ne laser operating at a wavelength of 632.8 nm, an avalanche photodiode detector with a high quantum efficiency, and an ALV/LSE-5003 multiple tau digital correlator electronics system.

2.4. Differential scanning calorimetry

For neat and blended samples the glass transition (T_g) was measured using a Thermal Analysis Instruments Q100 DSC under nitrogen at a flow rate of 50 mL/min. A heating rate of 10 °C/min was applied from room temperature to 230 °C. The samples were held at 230 °C for 1 min then quenched to 50 °C. A heating rate of 10 °C/min was applied until 230 °C, and the T_g was determined from the second heating scan by the temperature on the curve half way between the tangent lines drawn above and below the transition region.

2.5. Contact angle goniometry

Contact angle measurements were conducted via the sessile drop technique using a Rame'-Hart goniometer coupled with DROP-image® data analysis software. The static contact angle formed by drops of HPLC grade water (11 μL) and diidomethane (DiiM) (2 μL) was measured on each polymer surface immediately after deposition. Ten droplets of each test fluid were analyzed at different locations on each polymer surface. The solid-vapor surface energies (γ_{SV}) of the pure components and blends are calculated from the measured contact angles (θ) of water and diiodomethane on the polymer surfaces using the Owens–Wendt model given by Eq. (2) [28]. This model contains both a dispersive energy component (γ_{SV}^d) that accounts for van der Waals forces and a polar energy component (γ_{SV}^p) accounting for dipole–dipole, induced dipole and hydrogen bonding forces.

$$\gamma_{SV} = {\gamma_{SV}}^d + {\gamma_{SV}}^p \tag{2}$$

The polar and dispersive components of the Owens–Wendt model are found by combining Good's and Young's equations in Eq. (3), where the only unknowns are γ_{SV}^d and γ_{SV}^p. The contact angles of water and diiodomethane on each polymer surface are used to solve for the polar and dispersive energy components of each solid polymer surface by Eq. (3) [29].

$$(1+\cos\theta)\cdot\frac{{\gamma_{LV}}^p + {\gamma_{LV}}^d}{2\cdot{\gamma_L}^d} = \sqrt{{\gamma_{SV}}^d} + \sqrt{{\gamma_{SV}}^p}\cdot\sqrt{\frac{{\gamma_{LV}}^p}{{\gamma_{LV}}^d}} \tag{3}$$

In the above equation γ_L is the surface tension of the test fluid, and γ_{LV}^p and γ_{LV}^d are the polar and dispersive components of the surface tension of the test fluid.

2.6. Atomic force microscopy

AFM micrographs were collected with an Agilent 5500 AFM (Agilent Technologies, Santa Clara, CA) in alternating current mode using an etched silicon probe with a nominal resonant frequency of 275 kHz (RTESP, Veeco Instruments, Santa Barbara, CA). The scan rate was kept at 0.5 Hz, and images are an array of 512 × 512 data points. Data were processed using Gwyddion version 2.7 software to remove artifacts and improve image quality by applying plane leveling, line correction, and scar removal operations. AFM studies were performed under ambient conditions in a temperature (27 °C) and humidity (40–45%) controlled room. Multiple areas were imaged for each sample, and representative images are presented. Height and phase images of the pure component and blend surface morphologies were obtained on the film surfaces without further sample preparation. Measurements of root mean square roughness (R_{rms}) values were taken from AFM micrographs over an area of 625 μm^2 and calculated using Gwyddion version 2.7 software.

Bulk morphologies of blended systems were investigated by AFM analysis of microtomed surfaces. The films were embedded in a thermally cured epoxy resin. The cured epoxy surrounding the film was trimmed away to expose a small surface containing the film cross section. The surfaces were cut with a diamond knife using a microtome to obtain surfaces that were smooth on a nanoscopic level. After the cross sectional surface of the embedded film was located using an optical microscope, the cantilever was placed directly over the location, and height and phase micrographs were obtained simultaneously.

2.7. Nanoindentation

Hardness and reduced modulus values for all samples were calculated from load-displacement curves generated by displacement controlled indents using a Hysitron Triboindenter (Hysitron, Minneapolis, MN) with a Berkovich diamond probe tip. A trapezoidal displacement profile with a 5 s hold at the maximum displacement and displacement rate of 10 nm/s was applied to the samples. Ten indents were made in each specimen made at a maximum depth of 100 nm. The shape of the tip was modeled by making a series of indents in a fused quartz standard with depths ranging from 80 to 280 nm. Using the known value for the reduced modulus of fused quartz and the measured contact depth, h_c, area was fitted to a six parameter function of h_c using eqn. (4) to give the tip area function, $A(h_c)$, in nanometers by the relation:

$$A(h_c) = C_0{*}h_c^2 + C_1{*}h_c + C_2{*}h_c^{1/2} + C_3{*}h_c^{1/4} + C_4{*}h_c^{1/8} + C_5{*}h_c^{1/16} \tag{4}$$

where C_{0-5} are the parameters for the area function. Load-frame compliance was measured in a similar manner by making indents in a fused quartz standard. Total compliance is plotted versus $1/(P_{max})^{1/2}$, and the intercept is the load-frame compliance [30].

3. Results and discussion

3.1. Solution properties

In Fig. 2 static light scattering (SLS) data are linearly fitted using Zimm formalism, where K^*c/R_{theta} is plotted versus $\sin^2$(theta/2). There is good agreement for M_w from extrapolation of angular and concentration data, and parallel lines are observed at different concentrations and angles. The conformation of the polymer in solution can be determined from the angular dependence of light scattering from solution [31]. However, this method was not

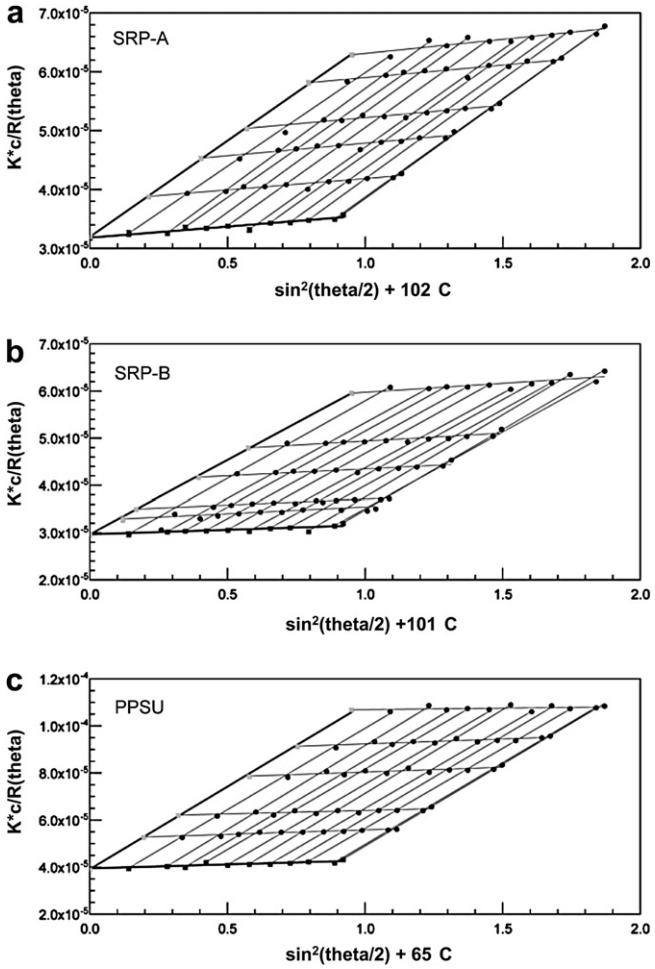

Fig. 2. Zimm plots: (a) SRP-A (b) SRP-B (c) PPSU.

applicable to the polymers under investigation because the angular variation of light scattering for rods and coils deviates significantly only at higher molecular weights. Therefore, dynamic light scattering (DLS) was employed to measure the hydrodynamic radius (R_h). The ratio of $<R_G>_z$ to R_h provides a measure of polymer conformation in solution [32]. The theoretical ratio ($<R_G>_z/R_h$) for a hard sphere is 0.778. Random coil polymers demonstrate ratios in the range of 1.27–2.05, while rod-like polymers show ratios greater than 2.2 [33–38].

Data from SLS and DLS are summarized in Table 1. SRP-A has an M_w of 32,000, SRP-B has a slightly higher molecular weight of 34,000 and the molecular weight of PPSU is 26,000. The $<R_G>_z/R_h$ values for the polymers indicate that each adopts a rodlike conformation when dissolved in NMP. SRP-A has the most extended conformation followed by PPSU and then SRP-B. SRP-A is expected to have a more extended conformation than SRP-B due to the greater number of para linkages between phenylene units in the copolymer backbone, while SRP-B contains a greater number of meta backbone linkages that reduce its degree of linearity. The reduced linearity in SRP-B results in a reduction in the $<R_G>_z$ in comparison to that of SRP-A, even though SRP-B has a greater molecular weight. The reduced degree of linearity of SRP-B is expected to provide an increased ability to form homogeneous blends with PPSU by increasing the free volume of the SRP phase. This increase in free volume relaxes the steric constraints associated with the SRP phase and helps prevent entropic demixing.

Table 1
Summary of SLS and DLS measurements for SRP-A, SRP-B, and PPSU.

	SRP-A	SRP-B	PPSU
M_w	32,000	34,000	26,000
$<R_G>_z$ (nm)	22.5	19.1	18.6
R_h (nm)	6.3	8.0	8.5
$<R_G>_z/R_h$	3.6	2.4	2.9
A_2 (mol*mL/g^2)	1.67×10^{-3}	1.59×10^{-3}	2.31×10^{-3}
χ_0	0.265	0.283	0.233

The second virial coefficient (A_2) measured from SLS is reported in Table 1. It reflects the strength of the interaction between the polymer and NMP and is used to calculate the polymer–solvent interaction parameter as concentration approaches zero (χ_o) of the system by the following relation [39]:

$$\chi_o = 0.5 - \rho^2 * V * A_2 \quad (5)$$

where ρ is the density of the polymer and V is the solvent molar volume. Polymer–solvent interaction decreases in the order PPSU > SRP-A > SRP-B. These results compare well with observations from dissolution of the polymers in NMP. PPSU dissolved in a short time at room temperature with stirring at a concentration of 10 g PPSU per 100 mL of solution. At the same concentration both SRPs required elevated temperatures to dissolve, but SRP-B required the most time. The increased solubility of SRP-A in NMP compared to SRP-B is explained by the higher benzoyl substitution in SRP-A which provides increased interaction with the solvent. The similarities of the χ_o values calculated from the A_2 indicate a low enthalpy of mixing for PPSU with SRP [40].

3.2. Bulk properties of pure components and blends

Blends were first assessed for miscibility by a visual inspection of films cast from blend solutions. PPSU, SRP-A and SRP-B polymers produce transparent, amorphous films when solution cast. The films are free standing with thicknesses greater than 25 μm. The difference in refractive index between PPSU and the SRPs is greater than 0.01, and thus a valid assumption concerning miscibility can be made by optical inspection [41,42]. Films prepared from blends containing PPSU and SRP-B appear transparent over the entire range of compositions, indicating that a homogeneous blend is produced during solution casting. Films prepared from blends containing PPSU and SRP-A are transparent at 20 wt% concentrations of the minor component, but those with an SRP-A content between 40 and 60 wt% have a cloudy appearance, indicating the presence of compositional heterogeneities.

The glass transition behavior of polymer blends is an indication of bulk blend miscibility. A single, well-defined glass transition is characteristic of a miscible blend, while multiple glass transitions indicate that the blend components possess phase separation or are only partially miscible [43]. Two conditions must be met for assessment of miscibility by a single glass transition. The blend must contain at least 10–20 wt% of the minor component, and the difference in the glass transition of the two components must be at least 20 °C [44,45]. Both of these conditions are satisfied in this study with the minor component content being greater than 20 wt% and the difference in the glass transitions between the SRP and PPSU being greater than 55 °C. Glass transition behavior is summarized in Table 2. Blends containing SRP-B and PPSU show a single, well-defined glass transition over the entire composition range, and blends of SRP-A and PPSU where the minor component is 20 wt% also show a single glass transition. Blends containing SRP-A and PPSU where the minor component content is approximately

Table 2
Glass transition behavior of neat and blended films cast from 10 wt% polymer solutions measured by DSC and their relation to the Fox equation.

Mass Fraction PPSU	Mass Fraction SRP-A	Mass Fraction SRP-B	Glass Transition (°C)	Predicted Glass Transition (°C)[a]
0.000	1.000	0.000	161	161
0.220	0.780	0.000	159	173
0.418	0.582	0.000	159, 210	184
0.623	0.377	0.000	160, 211	196
0.808	0.192	0.000	211	207
0.000	0.000	1.000	164	164
0.205	0.000	0.795	174	174
0.407	0.000	0.593	185	185
0.606	0.000	0.394	195	196
0.805	0.000	0.195	209	208
1.000	0.000	0.000	220	220

[a] Theoretical glass transition predicted by Fox equation.

40 wt% display two glass transitions indicating an immiscible blend.

A simple and convenient method to predict the temperature of the glass transition when there are weak polymer–polymer interactions is application of the Fox equation [46]:

$$1/T_g = w_1/T_{g1} + w_2/T_{g2} \quad (6)$$

where T_g is the glass transition temperature of the blend and w refers to the weight fraction. The subscripts 1 and 2 refer to the components of the blend. Blends of SRP-B and PPSU follow the Fox equation well, but those containing SRP-A and PPSU display significant deviations. Although blends containing SRP-A where the minor component is 20 wt% display a single T_g the actual temperature of the T_g is weighted towards the major component of the blend.

Microtomed samples were analyzed by AFM to investigate the bulk morphology of blended systems. AFM images of the SRP-A/PPSU film cross sections are shown in Fig. 3. These films exhibit bulk morphologies characteristic of metastable and unstable blends. The 20/80 (3a,b) and 80/20 (3g,h) SRP-A/PPSU blends display isolated regions of phase separated components that are dispersed in a predominantly homogeneous continuous phase. The 40/60 (3c,d) and 60/40 (3e,f) SRP-A/PPSU blends display co-continuous morphologies with larger phase dimensions [47]. Micrographs of the 40/60 and 60/40 SRP-B/PPSU blends are shown in Fig. 4. In contrast to the morphologies observed in the SRP-A/PPSU blends, the morphologies of SRP-B/PPSU blends appear homogeneous with no evidence of phase separation or compositional fluctuations.

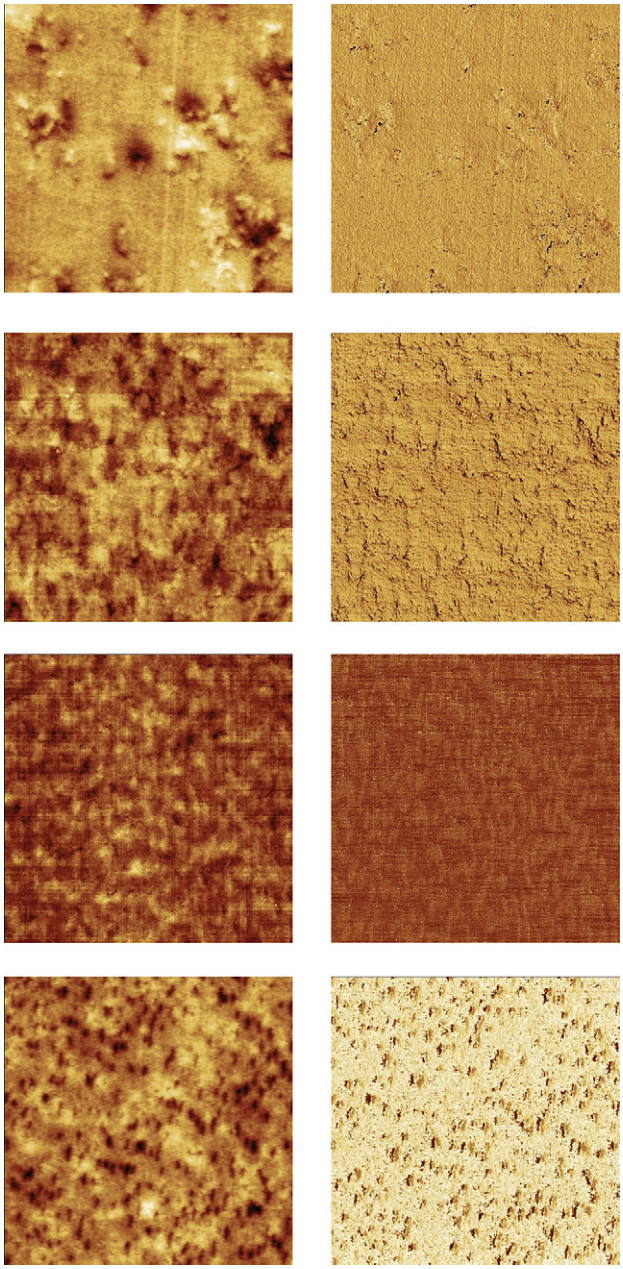

Fig. 3. AFM height (left) and corresponding phase (right) images of blends containing SRP-A and PPSU: (a) 20/80 SRP-A/PPSU, *Z*-scale = 30 nm; (b) 20/80 SRP-A/PPSU, *Z*-scale = 90°: (c) 40/60 SRP-A/PPSU, *Z*-scale = 20 nm; (d) 40/60 SRP-A/PPSU, *Z*-scale = 60°; (e) 60/40 SRP-A/PPSU, *Z*-scale = 15 nm; (f) 60/40 SRP-A/PPSU, *Z*-scale = 60°; (g) 80/20 SRP-A/PPSU, *Z*-scale = 30 nm; (h) 80/20 SRP-A/PPSU, *Z*-scale = 120°. The above images were taken on the cross sectional surfaces of the solution cast blends. Each image is 5 μm × 5 μm.

3.3. Surface properties of pure components and blends

The surface properties of polymer blends often deviate from those observed in the bulk. Differences in surface energy between the pure components of the blend lead to surface enrichment of the lower energy component. This phenomenon increases the concentration of one component at the surface and can induce phase separation in a metastable blend by creating large fluctuations in concentration over the polymer surface [48]. The measured contact angles, surface free energies and surface roughness (R_{rms}) values for the pure components and the blends are shown in Table 3. Standard deviations were calculated following propagation of uncertainty method and are shown in parenthesis next to the measurement or calculation.

SRPs exhibit slightly lower surface energy than PPSU indicating that a small driving force exists for surface enrichment of SRP in SRP/PPSU blends. The surface free energy of the blends is consistently lower than that of the pure components. Blends containing SRP-B and PPSU that displayed miscible characteristics according to bulk analysis techniques show only a small drop in surface free energy with respect to the pure components, while blends containing SRP-A and PPSU that displayed immiscible bulk characteristics display a significant drop in surface free energy.

The drop in surface free energy is correlated with surface roughness. Roughness and compositional heterogeneities present on blend surfaces can increase the observed contact angles of test fluids by inhibiting spreading, leading to a reduction in measured surface free energy [49,50]. The roughness induced by surface

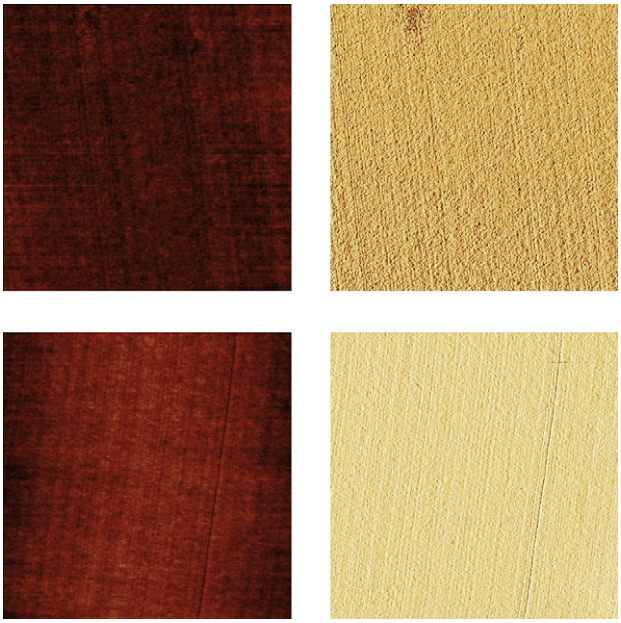

Fig. 4. AFM height (left) and corresponding phase (right) images of blends containing SRP-B and PPSU: (a) 40/60 SRP-B/PPSU, *Z*-scale = 20 nm; (b) 40/60 SRP-B/PPSU, *Z*-scale = 60°: (c) 60/40 SRP-B/PPSU, *Z*-scale = 20 nm; (d) 60/40 SRP-B/PPSU, *Z*-scale = 60°. The above images were taken on the cross sectional surface of the solution cast blends. Each image is 5 μm × 5 μm.

phase separation in SRP-A/PPSU blends (Fig. 7) is responsible for the lower measured surface free energy in these blends. SRP-B/PPSU blends (Fig. 6) have a lower degree of roughness and thus show only a moderate drop in surface free energy. The pure component surfaces (Fig. 5) have the lowest degree of surface roughness and are free of large compositional heterogeneities. The smooth, pure component surfaces give the most accurate assessment of the surface free energy.

The surface topographies of neat films of PPSU, SRP-A, and SRP-B are presented as AFM height images in Fig. 5. The different polymers exhibit similar surface morphologies with low degrees of R_{rms}. The surfaces are composed of predominantly homogeneous features with isolated heterogeneities, appearing as bright spots. In the homogeneous region of the surfaces the features are approximately 30–60 nm in diameter with heights ranging from 0.1 to 2 nm. The isolated heterogeneities are larger, having diameters ranging from 75 to 150 nm and heights on the order of 10 nm in each case. Due to the tight packing of the surface features in the neat films and the ratio of their diameter to height, it is apparent

Table 3
Contact angles, surface free energies, and roughness for pure polymers and blends.

	θ_{water} (deg.)	θ_{DiiM} (deg.)	γ_{SV} (mJ/m^2)	Roughness (nm)
Pure Components				
SRP-A	70.7(0.5)	29.5(1.7)	50.8(0.3)	0.60
SRP-B	71.3(0.8)	30.2(2.9)	50.3(0.5)	1.85
PPSU	70.1(0.5)	26.2(1.3)	52.0(0.5)	0.77
Blends				
20/80 SRP-A/PPSU	91.7(1.6)	54.0(2.0)	33.7(0.6)	10.9
40/60 SRP-A/PPSU	82.4(0.4)	26.2(1.0)	47.9(0.2)	10.7
60/40 SRP-A/PPSU	93.1(0.6)	56.6(1.1)	32.2(0.2)	5.09
80/20 SRP-A/PPSU	95.2(1.3)	56.2(2.0)	32.0(0.5)	1.64
20/80 SRP-B/PPSU	80.0(0.6)	26.1(0.7)	48.6(0.3)	0.72
40/60 SRP-B/PPSU	79.1(0.2)	25.1(0.6)	49.1(0.1)	0.71
60/40 SRP-B/PPSU	82.6(0.7)	27.5(1.5)	47.4(0.3)	0.92
80/20 SRP-B/PPSU	82.5(0.6)	27.4(1.6)	47.5(0.3)	1.93

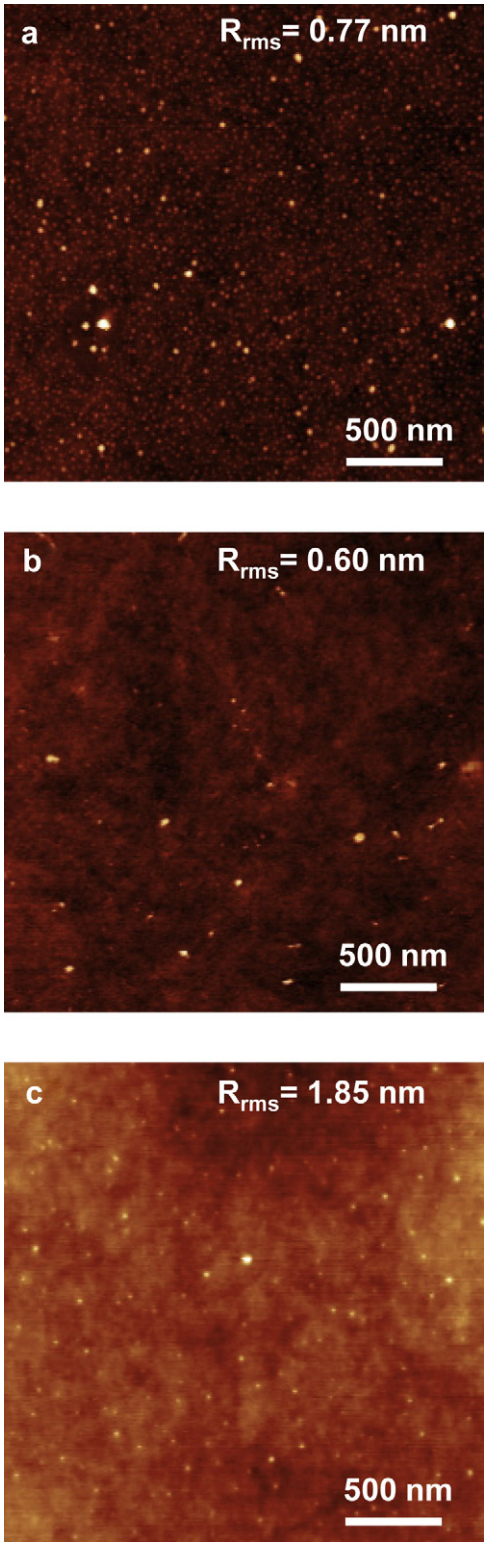

Fig. 5. AFM height images of neat polymer films: (a) PPSU (b) SRP-A (c) SRP-B. In all height images the vertical axis (*Z*-scale) is set to a 10 nm data scale.

that both homogeneous and heterogeneous features are not spherical, but possess either a cylindrical or disk shape. However, the distinction between cylinders and disks cannot be made without knowledge of the morphology below the surface, and the exact nature of the heterogeneities remains unknown. A possible

explanation is that they are nanoscopic crystallites that form on the surface during solution casting and are predominately composed of low molecular weight polymer species.

Blends of SRP-B and PPSU (Fig. 6) show surface morphologies similar to those of the pure components. Small bright features are observed, but there is no evidence of phase separation in the blends. These surfaces exhibit low degrees of roughness attributed to the small bright features rather than high levels of roughness caused by phase separation or metastability. These blends appear primarily homogeneous and display miscible characteristics.

Blends of SRP-A and PPSU demonstrate completely different surface morphologies that are strongly dependent upon blend composition, representative of metastable and immiscible blends. Fig. 7 shows AFM height images that are representative of the different morphologies exhibited for blends containing 20, 40, 60, and 80 wt% SRP-A. The blend containing 20 wt% SRP-A (Fig. 7a) has a continuous granular morphology with surface roughness of 10.9 nm. The granules show evidence of coalescence into structures having extended dimensions of 300–400 nm and widths of approximately 100 nm. Although the appearance of coalesced particles indicates the initial stages of phase separation, a clear interface between regions of SRP-A and PPSU is not apparent. When the fraction of SRP-A is increased to 40 wt% (Fig. 7b) phase separation is evident, and a clear interface is observed between domains of SRP-A and PPSU. This surface exhibits well defined island structures above a pitted surface. These islands have a height of up to 50 nm and diameters between 100 and 500 nm, while the pits are up to 200 nm wide with a depth of 30 nm. The 60 wt% SRP-A blend (Fig. 7c) displays a continuous, elevated surface with large pits, but no interface is observed between elevated regions and pits. The surface has an R_{rms} of 5.09 nm. The 80 wt% SRP-A (Fig. 7d) blend has a surface morphology and roughness similar to that of the pure components.

3.4. Nanomechanical properties of films

The experimental values for hardness (H) and reduced modulus (E_r) presented in Fig. 8 are calculated by the contact mechanics relationships developed by Oliver and Pharr [51]. The relationships for H and E_r are given by Eqs (7) and (8), respectively as:

$$H = P_{max}/A(h_c) \tag{7}$$

$$1/E_r = (\partial h_c/\partial P)*2*\left(\sqrt{A(h_c)}/\sqrt{\pi}\right) \tag{8}$$

where P is applied load, and P_{max} is the maximum applied load. The error bars associated with each data point represent one standard deviation based on ten indentation measurements. The anticipated degree of mechanical reinforcement, predicted by the rule of mixtures, is indicated by a solid line on each graph in Fig. 8. The linearity of the data for all systems in Fig. 8 indicates that their

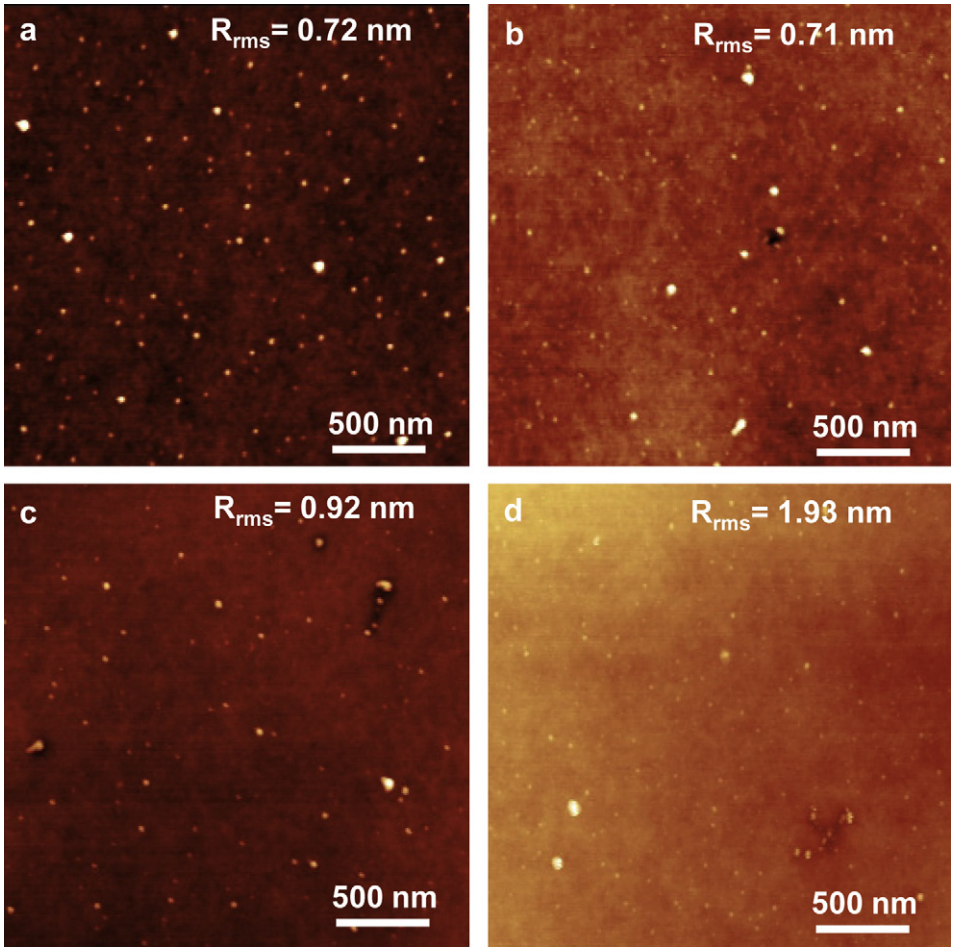

Fig. 6. AFM height images of solution cast polymer blends containing SRP-B and PPSU: (a) 20/80 SRP-B/PPSU, *Z*-scale = 10 nm; (b) 40/60 SRP-B/PPSU, *Z*-scale = 10 nm; (c) 60/40 SRP-B/PPSU, *Z*-scale = 20 nm; (d) 80/20 SRP-B/PPSU, *Z*-scale = 25 nm.

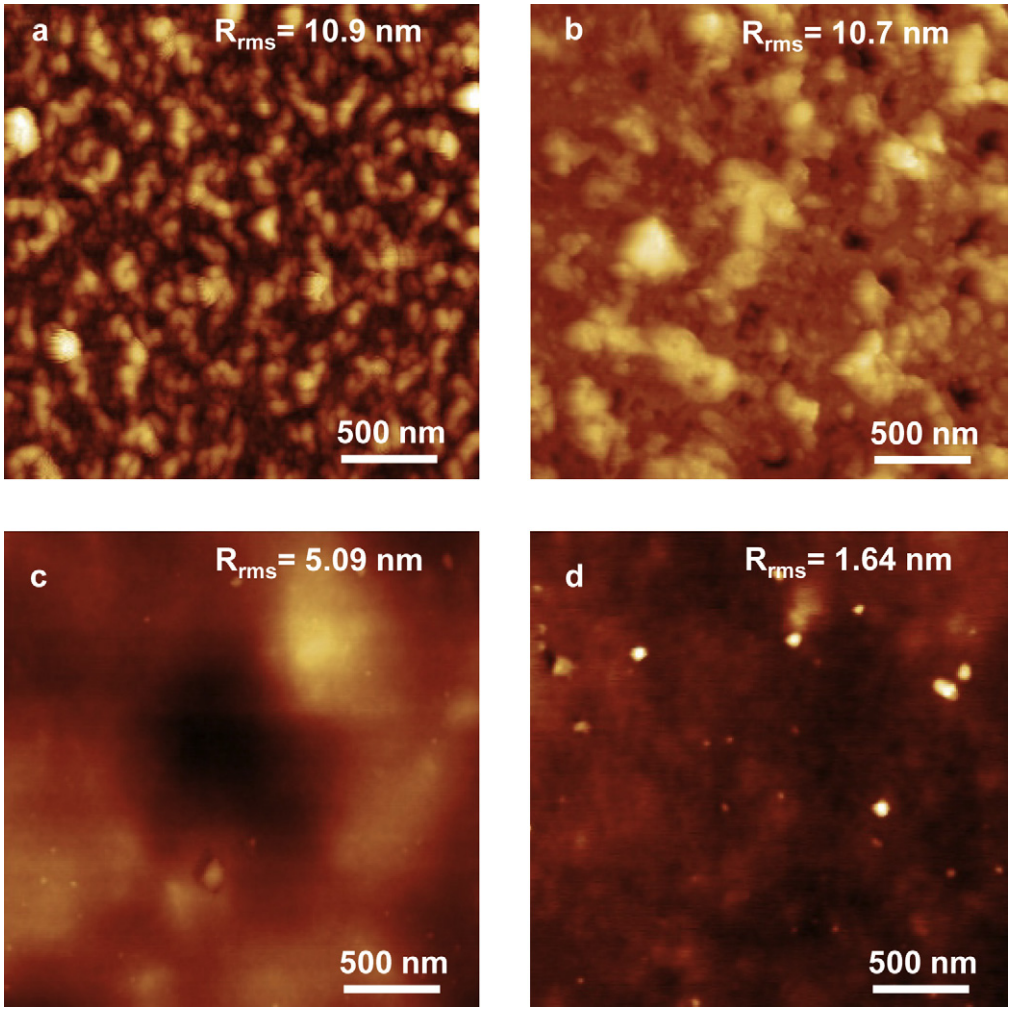

Fig. 7. AFM height images of solution cast polymer blends containing SRP-A and PPSU: (a) 20/80 SRP-A/PPSU, *Z*-scale = 75 nm; (b) 40/60 SRP-A/PPSU, *Z*-scale = 100 nm; (c) 60/40 SRP-A/PPSU, *Z*-scale = 50 nm; (d) 80/20 SRP-A/PPSU, *Z*-scale = 20 nm.

mechanical performance follows the rule of mixtures well. SRP-A has higher H and E_r than SRP-B, and blends containing SRP-A exhibit the same trend. The standard deviations associated with SRP-A blends are nearly two times greater than those observed for SRP-B blends, indicating higher surface heterogeneity for the SRP-A blends. The increase in surface heterogeneity indicates phase segregation of the SRP-A component at the surface. We explain this behavior by migration of the SRP during the final stages of solution casting. At the final temperature of solvent removal, 205 °C, the lower T_g SRPs are able to undergo long range segmental motion and are driven towards the surface.

3.5. Relation of copolymer structure to miscibility, morphology, and nanomechanics of blends

Light scattering measurements of A_2 and χ_o parameters revealed more similar values for SRP-A and PPSU than SRP-B and PPSU. Thus SRP-A is expected to have a lower enthalpy of mixing with PPSU than SRP-B. However, based on T_g measurements as well as bulk and surface morphology images, SRP-B is more compatible with PPSU than SRP-A. This can be explained in terms of chain conformation and flexibility. Light scattering measurements reveal that all three polymers adopt rod-like conformations in NMP, with SRP-A having the most extended conformation, followed by PPSU, and with SRP-B having the least extended conformation. The SRP backbone structure, formed by a combination of *meta*-phenylene and *para*-phenylene recurring units, possesses some degree of flexibility related to the number of meta linkages present. The PPSU molecule demonstrates increased flexibility due to the presence of sulfone and ether linkages in the backbone [10]. As the solution becomes concentrated PPSU deforms to accommodate restrictions placed on it by the highly rigid SRPs. From light scattering measurements the ratio of $<R_G>_z/R_h$ of SRP-B is much closer to PPSU than that of SRP-A. Blends containing SRP-A are more susceptible to entropic demixing. The more extended structure of SRP-A excludes PPSU from penetrating into the rigid phase by restricting the conformational freedom of PPSU. This leads to incompatible, heterogeneous blends of SRP-A and PPSU. SRP-B has a more kinked and less extended conformation that is more similar to that of PPSU than SRP-A. There is less restriction on the conformational freedom of PPSU leading to compatible, homogeneous blends.

Based on the lower surface energy calculated for the SRPs, surface enrichment of SRP is favored for the blends. Surface roughness and compositional heterogeneities lead to lower measured surface free energy for the blends in comparison to their pure components. AFM studies indicate surface enrichment of SRP-A in the solution cast films. In addition to surface free energy contributions, the method of solvent removal can have strong

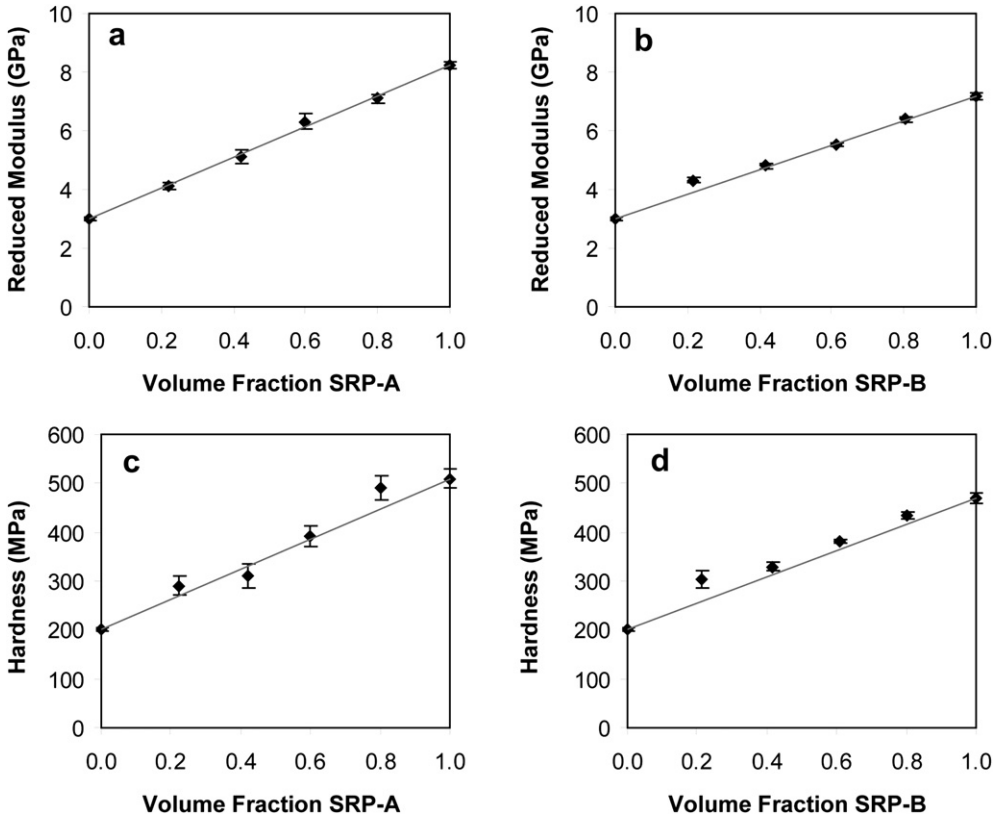

Fig. 8. Reduced modulus for (a) SRP-A/PPSU blends (b) SRP-B/PPSU blends and hardness for (c) SRP-A/PPSU blends (d) SRP-B/PPSU blends measured by nanoindentation. Error bars represent one standard deviation based on 10 measurements.

effects on the resulting morphology. In contrast to typical solution casting experiments, a high boiling point solvent is used in this system, and the casting procedure requires an extended time period at elevated temperatures. Initially, solvent removal is rapid and thermodynamically driven to reach vapor liquid equilibrium by reduced pressures. At this point polymer diffusion is limited, and the system can become locked in a state that deviates from thermodynamic equilibrium. Once the majority of the solvent has been removed, the residual solvent is removed by a diffusive mechanism that is controlled by temperature. At this point phase separation begins to occur in SRP-A blended systems. During this stage the high aspect ratio of SRP-A favors kinetic diffusion to form a separate phase from PPSU. Evidence for this is presented in both bulk and surface morphology images of SRP-A/PPSU blends. In contrast to SRP-A, the more kinked and lower aspect ratio SRP-B limits kinetic diffusion of the molecule, leading to more compatible and stable blends over the entire composition range, and homogeneous bulk and surface morphologies are observed for SRP-B/PPSU blends.

Phase segregation is further evidenced for SRP-A/PPSU blends by nanoindentation measurements. While all blends display exceptional nanomechanical performance that is closely predicted by the rule of mixtures, SRP-A blends exhibit substantially higher standard deviations in measured properties than SRP-B blends. Because of the scale of measurement, nanoindentation is sensitive to the degree of dispersion in a blend. Immiscible blends display regions that vary in local composition at the nano to micro level, while miscible blends have uniform composition and dispersion. For nanoindentation studies of a completely immiscible system, a bimodal distribution of mechanical properties is expected, with the average close to that predicted by the rule of mixtures. In contrast, homogeneous blends are expected to yield uniform distributions of property measurements with low standard deviations. This is evidenced by the phase-segregated SRP-A blends yielding standard deviations twice the level of those observed for the homogeneous SRP-B blends.

4. Conclusions

The molecular conformation, degree of linearity, and solubility of SRP and PPSU polymers in NMP were investigated by static and dynamic light scattering techniques. It was confirmed that the polymers exist as extended rods in solution, and NMP is a good solvent. In contrast to predictions based on the similarity of χ_o values, thermal analysis by DSC shows that SRP-B is more miscible with PPSU than SRP-A. This illustrates that the miscibility of these systems is driven by configurational entropy rather than intermolecular interactions. The higher aspect ratio, more rigid SRP-A copolymer formed phase separated and metastable blends with PPSU as observed in the bulk and surface morphology images from AFM. SRP-B copolymer, with its greater chain flexibility through higher meta-linkage content, formed a molecular composite. Phase separation in SRP-B/PPSU blends was not detected in the bulk or at the surface by AFM, and the blends appeared well mixed and homogeneous.

Surface segregation of the SRP-A copolymer was indicated through surface morphology and nanomechanical property characterization. The microstructure that develops below the surface in incompatible blends depends strongly upon blend composition and film formation methods. Study of the three dimensional morphologies produced in these systems revealed the complicated relationship between morphology and mechanical reinforcement, while probing localized features in the systems provided information

about local composition. The observed increase in mechanical properties at the surface of the films and development of complicated surface morphologies indicate the potential for the formation of PPSU/SRP blends that exhibit synergistic properties based on nano/microphase separation. Thermal, nanomechanical, and morphological characterization show that stable reinforced PPSU/SRP blends can be created and tailored through control of SPR copolymer architecture.

Acknowledgements

Partial funding from Solvay Advanced Polymers is gratefully acknowledged. This work was also supported by the major research instrumentation program of the National Science Foundation under Award Number DMR-0421403 and through instrumentation supported by the Office of Naval Research, Award No. N00014-07-1-1057.

References

[1] Lindenmeyer PH. Polym Eng Sci 1975;15:236–7.
[2] Krause SH, Haddock TB, Price GE, Adams WW. Polymer 1988;29:195–206.
[3] Venkatasubramian N, Dean DR, Dang TD, Price GE, Arnold FE. Polymer 2000;41:3213–26.
[4] Fukai T, Yang JC, Kyu T, Cheng SZD, Lee SK, Hsu SLC, et al. Polymer 1992;33(17):3621–6.
[5] Ballauf M, Dorgan JR. Polymer blends. In: Paul DR, Bucknall CB, editors. Formulation, vol 1. New York: Wiley; 2000. p. 200.
[6] Abe A, Flory PJ. Macromolecules 1978;11:1122–6.
[7] Ciferri A. Polym Eng Sci 1994;34:377–8.
[8] Hwang WF, Wiff DR, Benner CL, Helmeniak TE. J Macromol Sci Phys 1983;22:231–57.
[9] Flory PJ. Macromolecules 1978;11:1138–41.
[10] Flory PJ. Macromolecules 1978;11:1141–4.
[11] Bianchi E, Ciferri A, Conio G, Marsano E, Tealdi A. Macromolecules 1984;17:1526–31.
[12] Schartel B, Wendorff JH. Polym Eng Sci 1999;39:128–51.
[13] Trimmer MS, Wang Y, Marrocco ML, Lee VJ. US Patent 1999:5,886,130.
[14] Marrocco ML, Gagné RR, Trimmer MS. US Patent 1993:5,227,457.
[15] Marrocco ML, Trimmer MS, Hsu LC, Gagné RR. 39th Int SAMPE Symp 1994;39:1063–71.
[16] Morgan SE, Misra R, Jones PJ. Polymer 2006;47:2865–73.
[17] Thomas DB, Maljkovic N, Schuler T, Rushing T, Carter RL. Int Patent 2007:WO 2007/101852 A2.
[18] El-Hibri MJ, Myrick LJ, Thomas DB, Carter RL, Maljkovic N, Davis C, et-al. Int Patent 2007:WO 2007/101858 A2.
[19] El-Hibri MJ, Maljkovic N, Chavers RB, Massillon H. US Patent 20080312387.
[20] Yung HH, Scott SE, Thomas EL. Polymer 2001;42:6463–72.
[21] Robard A, Patterson D, Delmas G. Macromolecules 1977;10:706–8.
[22] Nandi AK, Mandal BM, Bhattacharyya SN. Macromolecules 1985;18:1454–60.
[23] Nishmoto M, Keskkula H, Paul DR. Polymer 1991;32:272–8.
[24] Ton-That C, Shard AG, Teare DOH, Bradley RH. Polymer 2001;42:1121–9.
[25] http://solvayadvancedpolymers.com [accessed 08 02 2009].
[26] Zimm BH. J Chem Phys 1945;13:141–5.
[27] Wyatt PJ. Analytica Chemica Acta 1993;272:1–40.
[28] Owens D, Wendt R. J Appl Polym Sci 1969;13:1741–7.
[29] Gurau V, Bluemle MJ, De Castro ES, Tsou YM, Mann A, Zawodzinski TA. J Power Sources 2006;160:1156–62.
[30] Triboindenter® users manual; NRL-M-011 v3.0. Minneapolis, MN: Hysitron Incorporated; 2003.
[31] Doty P, Bunce BH. J Am Chem Soc 1952;74:5029–34.
[32] Liu Y, Bo S. Chromatographia 2004;59:299–303.
[33] Burchard W, Schmidt M, Stockmayer WH. Macromolecules 1985;13:580–7.
[34] Rey A, Freire JJ, Garcia de la Torre J. Macromolecules 1987;20:342–6.
[35] Akcasu ZA, Benmouna M. Macromolecules 1978;11:1193–8.
[36] Reisman J, Kirkwood JG. J Chem Phys 1950;18:512–6.
[37] Mueller A, Buchard W. Colloid Polym Sci 1995;273:866–75.
[38] Savin G, Burchard W, Luca C, Beldie C. Macromolecules 2004;37:6565–75.
[39] Barton AF, editor. CRC handbook of polymer–liquid interaction parameters and solubility parameters. Boca Raton: CRC Press; 1990. p. 8.
[40] Gedde UW. Polymer physics. Dordrecht: Kluwer Academic Publishers; 2001. p. 72.
[41] Bohn L. In: Brandup J, Immergut EH, editors. Polymer handbook. New York: Wiley; 1975. p. III-211.
[42] Merfeld GD, Paul DR. Polymer blends. In: Paul DR, Bucknall CB, editors. Formulation, vol. 1. New York: Wiley; 2000. p. 55–92.
[43] Olabisi O, Robeson LM, Shaw MT. Polymer–polymer miscibility. New York: Academic Press; 1979.
[44] MacKnight WJ, Karasz FE, Fried JR. In: Paul DR, Newman S, editors. Polymer blends. New York: Academic Press; 1978.
[45] Karasz FE. In: Walsh DJ, Higgins JS, Maconnachie A, editors. Polymer blends and mixtures. Boston: Matinus Nijhoff Publishers; 1985.
[46] Fox TG. Bull Am Phys Soc 1956;1:123.
[47] Wen G, Li X, Liao Y. An L. Polymer 2003;44(14):4035–45.
[48] Jones RAL, Kramer EJ, Rafailovich MJ, Sokolov J, Schwartz SA. Phys Rev Lett 1986;62:280–3.
[49] de Gennes PG. Rev Mod Phys 1985;57:827–63.
[50] Dettre R, Johnson R. In: Fowkes FM, editor. Contact angle, wettability and adhesion. Washington D.C.: American Chemical Society; 1964.
[51] Oliver WC, Pharr GM. J Mater Res 1992;7:1564–83.